

# $^{89}\text{Zr}$ Immuno-PET: Comprehensive Procedures for the Production of $^{89}\text{Zr}$ -Labeled Monoclonal Antibodies

Iris Verel, MS<sup>1</sup>; Gerard W.M. Visser, PhD<sup>2</sup>; Ronald Boellaard, PhD<sup>3</sup>; Marijke Stigter-van Walsum, BS<sup>1</sup>; Gordon B. Snow, MD, PhD<sup>1</sup>; and Guus A.M.S van Dongen, PhD<sup>1</sup>

<sup>1</sup>Department of Otolaryngology/Head and Neck Surgery, VU University Medical Center, Amsterdam, The Netherlands; <sup>2</sup>Radionuclide Center, VU University, Amsterdam, The Netherlands; and <sup>3</sup>Department of Nuclear Medicine/PET Center, VU University Medical Center, Amsterdam, The Netherlands

The use of immuno-PET, the combination of PET with monoclonal antibodies (mAbs), is an attractive option to improve tumor detection and mAb quantification. The long-lived positron emitter  $^{89}\text{Zr}$  has ideal physical characteristics for immuno-PET, such as a half-life of 3.27 d, which is compatible with the time needed for intact mAbs to achieve optimal tumor-to-nontumor ratios. Thus far, a major limitation in the use of  $^{89}\text{Zr}$  has been the lack of suitable methods for its stable coupling to mAbs. In this article, practical protocols for reproducible isolation of highly pure  $^{89}\text{Zr}$  and the production of optimal-quality mAb- $^{89}\text{Zr}$  conjugates are provided. **Methods:**  $^{89}\text{Zr}$  was produced by a (p,n) reaction on natural yttrium ( $^{89}\text{Y}$ ), isolated with a hydroxamate column, and used for labeling of premodified mAbs. mAbs were premodified with a novel bifunctional derivative of the chelate desferrioxamine B (Df) via a new linker chemistry. To this end, Df was initially succinylated (*N*-sucDf), temporarily filled with Fe(III), esterified by use of tetrafluorophenol, and then directly coupled to mAbs. Chimeric mAb (cmAb) U36, directed against head and neck cancer, was used for *in vitro* and *in vivo* evaluation. The *in vitro* stability of cmAb U36-*N*-sucDf- $^{89}\text{Zr}$  was assessed in human serum, and its *in vivo* behavior was evaluated by biodistribution and PET imaging studies in tumor-bearing nude mice. A cmAb U36-Df- $^{89}\text{Zr}$  conjugate containing a previously described succinimide ring-thioether unit in the linker was used as a reference. **Results:**  $^{89}\text{Zr}$  was produced in large batches (6.5–13.5 GBq) and isolated with improved radionuclidic purity (>99.99%) and high yield (>94%). The Df-premodified mAbs gave  $^{89}\text{Zr}$ -labeling efficiencies of 80% within 30 min, resulting in conjugates with preserved integrity and immunoreactivity. With respect to stability, the novel cmAb U36-*N*-sucDf- $^{89}\text{Zr}$  conjugate appeared to be superior to the reference conjugate. *In vivo*, the novel conjugate demonstrated selective tumor targeting, and on PET images obtained at 24, 48, and 72 h after injection of this conjugate, small tumors in the range of 19–154 mg were readily visualized. **Conclusion:** Methods were developed for improved purification of the long-lived positron emitter  $^{89}\text{Zr}$ .

Moreover, a novel bifunctional Df chelate was synthesized for the reproducible coupling of  $^{89}\text{Zr}$  to mAbs. The suitability of such conjugates to detect millimeter-sized tumors in xenograft-bearing nude mice was demonstrated.

**Key Words:**  $^{89}\text{Zr}$ ; PET; radioimmunoconjugates; tumor detection; xenograft-bearing nude mice

**J Nucl Med 2003; 44:1271–1281**

**R**adiolabeled monoclonal antibodies (mAbs) have shown considerable potential for diagnosis and treatment of cancer (1,2). In recently performed clinical radioimmunoscinigraphy and radioimmunotherapy studies at our institute, the potential of the CD44 variant 6-specific mAb U36 for these purposes has been demonstrated (3,4). For the detection of head and neck squamous cell carcinoma (HNSCC), primary tumors as well as metastases, radioimmunoscinigraphy with  $^{99\text{m}}\text{Tc}$ -labeled mAb U36 IgG was found to be as valuable as the conventional imaging techniques CT and MRI, but the detection of tumor deposits smaller than 1 cm appeared to be a problem (3). Introduction of PET might further improve tumor detection because of its high resolution. In addition, PET has potential for quantitative imaging. These features should enable PET to provide proof of principle of antibody targeting and dosimetric determinations before radioimmunotherapy. For this purpose, we are focusing on the coupling of positron emitters to mAbs and the use of these radiolabeled mAbs in immuno-PET.

For a positron emitter to be appropriate for immuno-PET, it has to fulfill several requirements. Its physical half-life has to be compatible with the time needed for a mAb to achieve optimal tumor-to-nontumor ratios. For intact mAbs used for targeting solid tumors, this time is generally 2–4 d. Therefore, commonly used positron emitters such as  $^{11}\text{C}$  and  $^{18}\text{F}$  (half-lives of 20 and 110 min, respectively) are not suitable for labeling of mAbs. With respect to decay char-

Received Jul. 22, 2002; revision accepted Dec. 11, 2002.

For correspondence or reprints contact: Guus A.M.S. van Dongen, PhD, Department of Otolaryngology/Head and Neck Surgery, VU University Medical Center, De Boelelaan 1117, 1081 HV, Amsterdam, The Netherlands.

E-mail: gams.vandongen@VUmc.nl

acteristics, the positron-emitting isotope should by preference have no prompt  $\gamma$ -photons with an energy near 511 keV to optimize quantitative accuracy, and the  $\beta^+$ -energy should be as low as possible to obtain a high resolution. Besides this, production of the positron emitter should be easy (by preference with a medium-to-small cyclotron), reproducible, and of low cost. Finally, procedures should be available for stable coupling of the positron emitter to the mAb, with maintenance of the in vivo biodistribution characteristics of the latter.

Regarding the required half-life of several days, the 2 positron emitters  $^{124}\text{I}$  (half-life, 4.18 d) and  $^{89}\text{Zr}$  (half-life, 3.27 d) are most suitable. The low natural abundance of the target material for the production of  $^{124}\text{I}$ , however, requires enrichment into  $^{124}\text{Te}$  for a (p,n) or a (d,2n) reaction or into  $^{125}\text{Te}$  for a (p,2n) reaction. At the current stage of development, production of  $^{124}\text{I}$  is too expensive to allow routine clinical application. With respect to the latter,  $^{89}\text{Zr}$  can be produced by a (p,n) reaction on  $^{89}\text{Y}$ , an element that does not require enrichment because of its natural abundance of 100%. Taking the aforementioned considerations into account, we regard  $^{89}\text{Zr}$  ( $\beta^+ = 22.7\%$ , maximum  $\beta^+$  energy = 0.897 MeV) (Table 1) to be a promising candidate for immuno-PET.

The bifunctional chelate desferrioxamine B (Df) (Fig. 1) is the ideal chelate for binding of  $^{89}\text{Zr}$  because of the stable bond formation of  $^{89}\text{Zr}$  with the 3 hydroxamate groups of this chelate (6). For the coupling of this chelate to mAbs, Meijs et al. (7) modified the chelate into *N*-(*S*-acetyl)mercaptoacetyldesferrioxamine B (SATA-Df), and the lysine groups of the mAb were modified into maleimide groups. Upon reaction of these 2, a linker was formed containing a succinimide ring–thioether unit. At physiologic pH, the latter unit, however, might be responsible for the release of the chelate from the mAb as has, for example, been shown by Lewis and Shively (8) for their dodecanetetraacetic acid (DOTA)–conjugated mAbs. It can be anticipated that such instability will result in suboptimal delivery of  $^{89}\text{Zr}$  to the tumor.

In our group, good results have been obtained with a conjugation method based on the reaction of an active 2,3,5,6-tetrafluorophenol-chelate ester (TFP-chelate ester) with the lysine moieties of the mAb, resulting in a stable amide bond as the linker unit. This method gives optimal control over the number of groups conjugated to the mAb and has been used for the production of radioimmuno- and photoimmunoconjugates (9,10).

In the present report, we describe the use of this TFP ester

**TABLE 1**  
 $\gamma$ -Spectroscopic Analysis of  $^{89}\text{Zr}$  and Its Purification by Hydroxamate Column

Isotope	Half-life (d)	Main $\gamma$ -energies		Crude $^{89}\text{Zr}$ solution* (% activity $\pm$ SD)	Waste fractions <sup>†</sup> (% activity $\pm$ SD)	Purified $^{89}\text{Zr}$ solution <sup>‡</sup> (% activity $\pm$ SD)
		MeV	% Abundance <sup>§</sup>			
$^{89}\text{Zr}$	3.27	0.511	45.3	99.98 $\pm$ 0.0045	1.0 $\pm$ 1.0	97.0 $\pm$ 3.3
		0.909	99.9			
		1.202	0.014 <sup>  </sup>			
		1.622	0.070 <sup>  </sup>			
		1.657	0.100			
		1.713	0.769			
		1.744	0.130			
$^{88}\text{Zr}$	83.4	0.393	100	1.5 $\pm$ 1.8 $\times 10^{-4}$	1.2 $\pm$ 2.3 $\times 10^{-6}$	2.2 $\pm$ 2.2 $\times 10^{-4}$
$^{88}\text{Y}$	106.64	0.898	93.4	6.0 $\pm$ 5.1 $\times 10^{-5}$	6.2 $\pm$ 5.5 $\times 10^{-5}$	ND
		1.836	99.3			
$^{48}\text{V}$	16.24	0.511	100	2.9 $\pm$ 0.3 $\times 10^{-3}$	3.1 $\pm$ 0.3 $\times 10^{-3}$	ND
		0.984	100			
		1.312	97.5			
$^{56}\text{Co}$	78.76	0.511	39.7	8.9 $\pm$ 4.4 $\times 10^{-4}$	9.7 $\pm$ 4.3 $\times 10^{-4}$	ND
		0.847	99.9			
		1.238	67.0			
$^{65}\text{Zn}$	243.9	0.511	2.92	7.1 $\pm$ 4.1 $\times 10^{-3}$	6.9 $\pm$ 5.3 $\times 10^{-3}$	ND
		1.116	50.7			
$^{156}\text{Tb}$	5.34	0.199	37.4	2.6 $\pm$ 0.5 $\times 10^{-3}$	3.3 $\pm$ 0.5 $\times 10^{-3}$	ND
		0.534	61.2			
		1.222	29.4			

\*Total amount of activity found in crude solution is set at 100%; data are mean  $\pm$  SD of 5 productions.

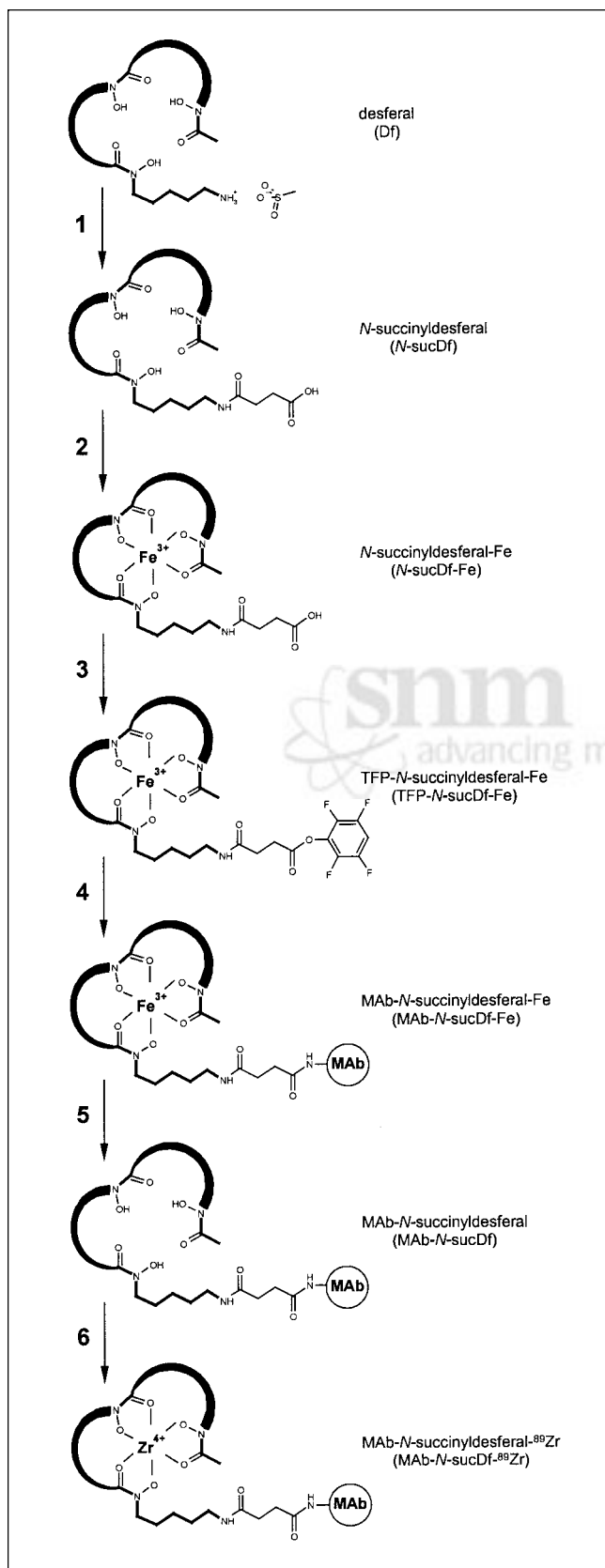
<sup>†</sup>Consisting of flow-through (after loading crude  $^{89}\text{Zr}$  solution onto hydroxamate column), HCl fraction, and water fraction.

<sup>‡</sup>Consisting of five 1 mol/L oxalic acid fractions of 0.5 mL.

<sup>§</sup>Complete list of found  $\gamma$ -energies of  $^{89}\text{Zr}$ ; resulting from 22.7%  $\beta^+$  abundance, maximum  $\beta^+$  energy = 0.897 MeV.

<sup>||</sup>These data are from this study;  $\gamma$ -energies with abundance of 0.1% or higher were found to be in full accordance with  $\gamma$ -energies reported by International Commission on Radiological Protection (5).

ND = not detectable, i.e., below 10 Bq.



approach for the improved purification of  $^{89}\text{Zr}$  as well as for the coupling of a novel bifunctional derivative of Df to mAbs. The *in vitro* stability of these  $^{89}\text{Zr}$ -conjugates and their biodistribution in xenograft-bearing nude mice were determined and compared with succinimide ring–thioether linked Df- $^{89}\text{Zr}$  conjugates. The feasibility of visualizing millimeter-sized tumors was demonstrated in HNSCC-bearing nude mice.

## MATERIALS AND METHODS

### mAbs

Selection, production, and characterization of chimeric mAb (cmAb) U36, as well as of the control murine mAbs (mmAbs) 425 and E48, have been described elsewhere (10).

### $^{89}\text{Zr}$ Production and Purification

$^{89}\text{Zr}$  was produced by a (p,n) reaction on natural yttrium ( $^{89}\text{Y}$ ). For this purpose, an  $^{89}\text{Y}$ -target was bombarded with 14 MeV

**FIGURE 1.** Schematic representation of premodification and postlabeling of mAbs with  $^{89}\text{Zr}$ . Step 1 is synthesis of *N*-sucDf, as described in Materials and Methods. Step 2 is complexation of *N*-sucDf with Fe(III). *N*-sucDf (9 mg, 13.6  $\mu\text{mol}$ ) is dissolved in 3 mL of 0.9% NaCl, containing 60  $\mu\text{L}$  of 0.1 mol/L  $\text{Na}_2\text{CO}_3$  (final pH 6.5–7.0). To this solution, 300  $\mu\text{L}$  (14.8  $\mu\text{mol}$ ) of  $\text{FeCl}_3$  solution (8 mg/mL in 0.1 mol/L HCl) is added. Step 3 is esterification of *N*-sucDf-Fe. After 10 min, to *N*-sucDf-Fe solution are added 300  $\mu\text{L}$  (0.36 mmol) of TFP solution (200 mg/mL in MeCN) and 120 mg (0.63 mmol) of solid EDC (final pH 5.8–6.0). After 45 min of incubation, reaction mixture is loaded onto conditioned Sep-Pak  $\text{C}_{18}$  cartridge (Waters), followed by washing with 60 mL of sterile water for injection. TFP-*N*-sucDf-Fe is eluted from Sep-Pak cartridge with 1.5 mL of MeCN. Step 4 is conjugation of TFP-*N*-sucDf-Fe to mAb. To 1 mL (33 nmol) of mAb solution (5 mg/mL), pH 9.5–9.8 (adjusted with 0.1 mol/L  $\text{Na}_2\text{CO}_3$ ), 20  $\mu\text{L}$  (63 nmol) of TFP ester solution (2.5 mg/mL in MeCN) are added to obtain final chelate:mAb ratio of 1:1 (based on 54% reaction efficiency). After 30 min, 2 times 25  $\mu\text{L}$  of gentisic acid solution (100 mg/mL in 0.32 mol/L  $\text{Na}_2\text{CO}_3$ ) are added to reaction mixture and pH is adjusted to 4.3–4.5 with 4 times 6  $\mu\text{L}$  of 0.25 mol/L  $\text{H}_2\text{SO}_4$ . Step 5 is removal of Fe(III) from mAb-*N*-sucDf-Fe. To reaction mixture, 50  $\mu\text{L}$  (3.3  $\mu\text{mol}$ ) of an EDTA solution (25 mg/mL) is added and solution is incubated for 30 min at 35°C (final pH 4.3–4.5). After 30 min, EDTA, TFP, iron (as  $[\text{Fe}(\text{III})\text{EDTA}]$ ), and unreacted hydrolyzed ester (*N*-sucDf) are removed by gel filtration using PD-10 column (eluent: 0.9% NaCl/gentisic acid [5 mg/mL], pH 5): First 2.6 mL (containing reaction volume and first 1.5 mL) are discarded, and modified mAb is collected in next 2 mL. Step 6 is labeling of mAb-*N*-sucDf with  $^{89}\text{Zr}$ . To 600  $\mu\text{L}$  of  $^{89}\text{Zr}$  oxalic acid solution (1 mol/L oxalic acid), 130  $\mu\text{L}$  of 0.9% NaCl, 270  $\mu\text{L}$  of 2 mol/L  $\text{Na}_2\text{CO}_3$ , and 3 mL of 0.5 mol/L HEPES (pH 7.2–7.4) are added, followed by 2 mL (33 nmol) of modified mAb solution (2.5 mg/mL in 0.9% NaCl/gentisic acid [5 mg/mL], pH 5), final pH 7.2–7.4. Reaction volume can be varied provided amounts of oxalic acid,  $\text{Na}_2\text{CO}_3$ , and HEPES buffer are adjusted accordingly. After 30 min, reaction mixture (6 mL) is divided over 3 PD-10 columns (eluent: 0.9% NaCl/gentisic acid [5 mg/mL], pH 5): First 2.5 mL (2-mL sample volume and first 0.5 mL) are discarded, and radiolabeled mAb is collected in next 3 mL. Bold arches represent  $-(\text{CH}_2)_2\text{CONH}(\text{CH}_2)_5-$ . Desferal (Df) (Novartis) is term used instead of desferrioxamine B, and Df-Fe is term used to represent corresponding iron(III) complex (ferrioxamine).

protons (11) for 2–3 h (65–80  $\mu\text{A}$ ) while the target support was cooled with water (AVF cyclotron; Philips).  $^{89}\text{Y}$  targets were prepared by sputtering an  $^{89}\text{Y}$  layer (35  $\mu\text{m}$ ; Highways International) on a copper support (Mallinckrodt Medical) as described by Meijs et al. (12). After irradiation, the  $^{89}\text{Y}$  layer was slowly dissolved in 4 successive 0.5-mL portions of 1 mol/L HCl (Sigma-Aldrich). Then,  $^{89}\text{Zr}$  was oxidized to the IV-oxidation state with 0.1 mL hydrogen peroxide (30% v/v; Mallinckrodt Baker), and 0.22 mL of 12 mol/L HCl was added to set the final HCl concentration at 2 mol/L. After 1 h,  $^{89}\text{Y}$  and radionuclidic impurities were removed using a hydroxamate column.

Hydroxamate column material for purification of  $^{89}\text{Zr}$  was prepared from Accell Plus CM cation exchange medium (300  $\text{\AA}$ , 0.35 mmol/g ligand density; Waters). To ensure a reproducible high level of hydroxamate function, a new 2-step ester-mediated method was developed. In the first reaction step, the carboxylic acid groups of the cation exchange medium were esterified using an excess of TFP (Acros Organics) and 1-ethyl-3-(3-dimethylaminopropyl)-carbodiimide (EDC; Acros Organics). For an optimal conversion of carboxylic acid groups into ester groups, the TFP and EDC were added in 2 successive portions. In short: To 1 g of Accell, suspended in 8 mL of water for injection (Baxter), 75  $\mu\text{L}$  of 3 mol/L HCl, 1 mL of a TFP solution (200 mg/mL in MeCN, 1.2 mmol), and 384 mg of solid EDC (2 mmol) were added (final pH 5.7–6.0). The suspension was mixed end over end for 1 h. Afterward, 105  $\mu\text{L}$  of 3 mol/L HCl were added, along with a new 1-mL portion of TFP and a new 384-mg portion of EDC (final pH 5.7–6.0). After 1 h of mixing, the material was washed with 30 mL of MeCN to remove EDC, its corresponding urea-reaction product, and unreacted TFP.

In the second reaction step, hydroxamate groups were introduced on the resin via the reaction of the ester groups with an excess of hydroxylamine hydrochloride (Aldrich). The hydroxylamine hydrochloride solution was prepared by adding 690 mg (10 mmol) of hydroxylamine hydrochloride to a mixture of 1 mL of 1 mol/L NaOH and 2 mL of MeOH, followed after 5 min by the addition of 1 mL of 1 mol/L NaOH to bring the pH to 5.3–5.4. This solution was added to the esterified resin (final pH 5.1–5.2) and mixed overnight at room temperature. The column material was washed thoroughly with 140 mL of water for injection and 70 mL of MeCN, respectively, and dried in vacuo (freeze-drying). The material can be stored for at least 4 mo without any decrease of  $^{89}\text{Zr}$ -binding capacity (extended storage periods are under investigation). For the preparation of a hydroxamate column, an Extract-Clean tube (1.5 mL; Alltech) with a frit placed at the bottom (pore size, 20  $\mu\text{m}$ ) was packed with a suspension of 100 mg of hydroxamate column material in 0.9% NaCl (Baxter). After application of the  $^{89}\text{Zr}$ -target solution and the eluting solvents, the flow of solvents was initiated by connecting vacuum tubes (Vacutainers without additives; Becton Dickinson) to the column with a needle (0.6 mm  $\times$  25 mm).

Before use, a hydroxamate column was equilibrated with 5 mL of MeCN, followed by 10 mL of 0.9% NaCl and, finally, 2 mL of 2 mol/L HCl. After loading of the  $^{89}\text{Zr}$ -target solution onto the column, the column was rinsed with 6 mL of 2 mol/L HCl and 6 mL of sterile water for injection, respectively. Under these conditions,  $^{89}\text{Zr}$  and the trace amount of  $^{88}\text{Zr}$  remained bound to the resin, whereas  $^{89}\text{Y}$  and the radionuclidic metal impurities were eluted. The zirconium isotopes were eluted with 5 successive portions of 0.5 mL of 1 mol/L oxalic acid (Aldrich). In general, the

oxalic acid fractions contained successively 40%, 40%, 10%, 5%, and 2% of the applied radioactive zirconium.

#### Preparation of mAb-*N*-Succinyl-desferrioxamine B- $^{89}\text{Zr}$

mAbs were premodified with a novel bifunctional derivative of the chelate Df (*N*-sucDf) via an amide linkage and subsequently labeled with  $^{89}\text{Zr}$  (Fig. 1).

The chelate Df was converted into *N*-succinyl-desferrioxamine B (*N*-sucDf) in step 1 according to a modified procedure of Herscheid et al. (13). In short: 1.7 g of succinic anhydride (17 mmol; Baker Chemicals) were added to 7.5 mL of pyridine (Sigma-Aldrich Chemie) containing 0.5 g of Df (0.76 mmol; Novartis). The solution was stirred for 24 h at room temperature and added to 120 mL of 0.15 mol/L NaOH. After additional stirring for 16 h at room temperature, the pH was adjusted to 2 with 12 mol/L HCl and cooled for 2 h at 4°C. The precipitate was thoroughly washed with 500 mL of 0.01 mol/L HCl, and the white product was dried in vacuo (freeze-drying).

Coupling of *N*-sucDf to mAbs and labeling with  $^{89}\text{Zr}$  is schematically represented in steps 2 through 6 of Figure 1. In short, the hydroxamate groups of *N*-sucDf were temporarily blocked with Fe(III) in step 2, *N*-sucDf-Fe was esterified with TFP in step 3, and TFP-*N*-sucDf-Fe was coupled to mAbs in step 4. Thereafter, Fe(III) was removed by transchelation to ethylenediaminetetraacetic acid (EDTA) (formation of  $[\text{Fe(III)EDTA}]^-$  (14)) in step 5, and mAb-*N*-sucDf was labeled with  $^{89}\text{Zr}$  in step 6.

#### Preparation of mAb-SMCC-SATA-Df- $^{89}\text{Zr}$

As reference to the new method for  $^{89}\text{Zr}$  labeling (as depicted in Fig. 1), Df was also coupled to mAbs via a thioether linkage as previously described by Meijs et al. (7). In short, the amine group of Df was reacted with *N*-succinimidyl-S-acetylthioacetate (SATA; Pierce). Modification of mAb-lysine groups into maleimide groups was performed by reaction with sulfosuccinimidyl 4-(*N*-maleimidomethyl)cyclohexane-1-carboxylate (sulfo-SMCC; Pierce); the number of maleimide groups per mAb molecule was 0.8–0.9 as determined chemically with Ellman's reagent (7). mAb-SMCC was purified by the use of a 10DG column (Bio-Rad). After incubation of the purified mAb-SMCC sample with SATA-Df (activated in 0.1 mol/L  $\text{Na}_2\text{CO}_3$ ) for 90 min, unreacted maleimide groups were quenched with an excess of hydroxylamine for 15 min. Purification and labeling of the thus modified mAb with  $^{89}\text{Zr}$  and the subsequent purification of the conjugate were performed essentially the same as described for the novel procedure (Fig. 1, steps 5 and 6).

#### Analyses

A Ge(Li) detector coupled to a multichannel analyzer was used to quantify  $^{89}\text{Zr}$ , to monitor  $^{89}\text{Zr}$  purification, and (after decay of most of  $^{89}\text{Zr}$ ) to identify and quantify radionuclidic impurities (Table 1). For quantification of  $^{89}\text{Zr}$  activities in a dose calibrator, the  $^{54}\text{Mn}$  mode was used, multiplying the displayed amount of activity by a factor of 0.67. Quantification in a  $\gamma$ -counter (LKB Wallac 1282 CompuGamma; Pharmacia) was performed on the 909-keV  $\gamma$ -energy of  $^{89}\text{Zr}$  (efficiency, 21.7%). Samples of the  $^{89}\text{Zr}$  oxalic acid fractions and of the purified mAb- $^{89}\text{Zr}$  solution were analyzed for the presence of any remaining  $^{89}\text{Y}$  by particle-induced x-ray emission (PIXE) according to the method described by Vis et al. (15).

High-performance liquid chromatography (HPLC) was performed to monitor the Df derivatives, the chemically modified mAbs, and the radiolabeled mAbs. *N*-sucDf, *N*-sucDf-Fe, and

TFP-*N*-sucDf-Fe were analyzed with a Chromspher 5 C18 column (250 × 4.6 mm; Chrompack) with a gradient elution. Solvent A consisted of 10 mmol/L sodium phosphate, pH 6, and solvent B of 100% MeCN. The gradient was as follows (flow rate, 1 mL/min): 5 min of 100% A, linear increase of eluent B to 35% during 25 min, 10 min of 35% B. HPLC analysis of the chemically modified mAbs and the radiolabeled mAbs was performed as described before (10). mAb compounds were monitored by ultraviolet absorbance at 280 nm, Df compounds at 215 nm, and Df-Fe(III) complexes at 430 nm, whereas radiolabeled compounds were monitored either by continuous radioanalytic detection or by measurement of collected fractions. The equipment used has been described before (10).

HPLC analyses of PD-10 column (Pharmacia Biotech) elution profiles were performed as described before (16). Profiles of EDTA, *N*-sucDf, and TFP (Fig. 1, step 5) were determined with a gradient elution by ultraviolet absorbance at 210 nm. Solvent A consisted of 10 mmol/L sodium phosphate, pH 6, and solvent B of 100% MeCN. The gradient was as follows (flow rate, 1 mL/min): 2 min of 100% A, linear increase of eluent B to 40% during 13 min, 5 min of 40% B (retention times of 2.9, 12.3, and 15.6 min, respectively). Oxalic acid and *N*-2-hydroxyethylpiperazine-*N'*-2-ethanesulfonic acid (HEPES) (Fig. 1, step 6) were analyzed by HPLC with 10 mmol/L sodium phosphate, pH 6, as eluent, a flow rate of 0.4 mL/min (retention times of 6.2 and 7.8 min, respectively), and a wavelength of 210 nm. For determination of the PD-10 column elution profile of [Fe(III)EDTA]<sup>-</sup>, <sup>59</sup>Fe (370 MBq/mL in 0.5 mol/L HCl; Amersham Pharmacia Biotech) was used as tracer and the fractions were counted with a  $\gamma$ -counter.

For the measurement of the serum stability of radioimmunoconjugates, samples were incubated in freshly prepared human serum (1:1 v/v dilution) at 37°C in a humidified incubator maintained at 5% CO<sub>2</sub> and 95% air. Radioimmunoconjugates were also incubated in heat-inactivated serum (treated for 40 min at 56°C); in 20% human serum albumin (HSA), pH 7.2 and 9.0; and in 20% HSA, pH 9.0, supplemented with an excess of L-cysteine (9  $\mu$ mol/mL). At various intervals, samples were taken and analyzed by HPLC.

Radiochemical purity and integrity of the radiolabeled mAbs were monitored by instant thin-layer chromatography (ITLC) (eluent: citric acid, 20 mmol/L, pH 5), sodium dodecylsulfate-polyacrylamide gel electrophoresis (SDS-PAGE) and analysis by a PhosphorImager (Molecular Dynamics), and immunoreactivity determination as previously described (9,10).

### Animal Studies

For the biodistribution and PET studies, female nude mice (athymic nu/nu, 23–32 g, 8–10 wk old; Harlan CPB) bearing human HNX-OE xenografts were used. HNX-OE xenografts were established after subcutaneous injection of HNSCC cell-line VU-SCC-OE (17) and repeated transplantation as xenografts in nude mice. Two to 3 wk after implantation, the mice were used for experiments. All animal experiments were performed according to the U.S. National Institutes of Health principles of laboratory animal care (18) and the Dutch national law “Wet op de Dierproeven” (Stb 1985, 336).

For the biodistribution study, mice (tumor size, 30–200 mg) were anesthetized with ether, and 0.37 MBq cmAb U36-*N*-sucDf-<sup>89</sup>Zr (100  $\mu$ L, 100  $\mu$ g mAb) or 0.37 MBq of the reference conjugate cmAb U36-SMCC-SATA-Df-<sup>89</sup>Zr (100  $\mu$ L, 100  $\mu$ g mAb) was injected into the retroorbital plexus. The specific activities of

the radioimmunoconjugates were 41 MBq/mg and 39 MBq/mg, respectively, and unlabeled mAb was added to bring the total mAb dose to 100  $\mu$ g per mouse. At indicated times after injection, the mice were anesthetized, bled, killed, and dissected. After blood, tumor, normal tissues, and gastrointestinal contents were weighed, the amount of radioactivity in each was measured in a  $\gamma$ -counter. Radioactivity uptake was calculated as the percentage of the injected dose per gram of tissue (%ID/g). Differences in tissue uptake between groups were statistically analyzed with the Student *t* test for unpaired data. Differences were considered significant for *P* < 0.05.

PET studies were performed using a prototype single-crystal-layer HRRT 3-dimensional PET scanner (CTI). The axial field of view of the PET scanner is 25.5 cm, and the transaxial field of view is 31.2 cm; radial and transaxial resolutions are 2.6 mm in full width at half maximum at the center of the field. Transmission scans for attenuation correction were obtained in 2-dimensional mode (consisting of 52 scans, using a 740-MBq <sup>137</sup>Cs point source), and emission scans were obtained in 3-dimensional mode. Images were reconstructed by filtered backprojection and consisted of 207 image planes of 256 × 256 pixels, and each voxel equaled 1.21 × 1.21 × 1.21 mm.

Mice bearing HNX-OE xenografts (19–154 mg) were anesthetized with ether and injected with 3.7 MBq cmAb U36-*N*-sucDf-<sup>89</sup>Zr (109 MBq/mg, 250  $\mu$ L, 100  $\mu$ g mAb). Before scanning, the mice were anesthetized with sodium pentobarbital (75 mg/kg, intraperitoneal) and positioned in the PET scanner. A transmission scan of 380 s was followed by a 60-min emission scan. Mice were scanned and then immediately dissected at 24 h (2 mice), 48 h (2 mice), and 72 h (6 mice) after injection. In addition, 2 mice were scanned 3 times: at 24, 48, and 72 h after injection; after 72 h these mice were dissected. Activity in tumors at the time of scanning was quantified by Ge(Li) and in a  $\gamma$ -counter together with a standard.

## RESULTS

### Production and Purification of <sup>89</sup>Zr

After irradiation, the <sup>89</sup>Y-layer was dissolved and the amount of <sup>89</sup>Zr was determined, as well as that of contaminating radionuclides (Table 1). The crude yield of <sup>89</sup>Zr was between 6.5 and 13.5 GBq (110–190 min of irradiation), with less than 1.3–2.7 MBq (0.02%, Table 1) of radionuclidic impurities. A small amount (0.00015%) of <sup>88</sup>Zr was observed, being the result of a (p,2n) reaction on <sup>89</sup>Y. The isotope <sup>88</sup>Y is formed as a daughter product from <sup>88</sup>Zr and possibly from a (p,pn) reaction on <sup>89</sup>Y. The isotope <sup>65</sup>Zn is formed by a (p,n) reaction on the copper support, whereas <sup>48</sup>V, <sup>56</sup>Co, and <sup>156</sup>Tb are formed on titanium, iron, and gadolinium impurities, respectively, in the <sup>89</sup>Y-target. Removal of the bulk nonradioactive <sup>89</sup>Y and of the radionuclidic impurities <sup>88</sup>Y, <sup>48</sup>V, <sup>56</sup>Co, <sup>65</sup>Zn, and <sup>156</sup>Tb (except <sup>88</sup>Zr) was achieved with a hydroxamate column (Table 1). As a result, more than 99.99% pure <sup>89</sup>Zr was obtained in 1 mol/L oxalic acid, with an overall yield of 97.0% ± 3.3%. PIXE analysis of the isolated <sup>89</sup>Zr oxalate revealed the absence of nonradioactive <sup>89</sup>Y.

### Preparation of mAb-*N*-sucDf-<sup>89</sup>Zr

Step 1 in the preparation of mAb-*N*-sucDf via the TFP ester approach, as depicted in Figure 1, is the carboxylation of the primary amine of Df. After isolation of the product, *N*-sucDf was obtained in a yield of 68%–73%. After temporary blocking of the hydroxamate groups of *N*-sucDf with Fe(III) in step 2 (<sup>59</sup>Fe was used as a tracer to facilitate analytic monitoring) and nearly quantitative esterification (Figs. 2A and 2B), TFP-*N*-sucDf-Fe was isolated by a Sep-Pak (Waters) procedure in yields of about 80% in step 3. The TFP ester could be stored for at least 8 wk in MeCN at -70°C (data not shown).

Conjugation conditions selected for the technical protocol comprised the addition of 63 nmol of ester to 33 nmol of mAb in step 4. For cmAb U36, mmAb E48, and mmAb 425, these conditions resulted in a reproducible conjugation efficiency of 54% ± 5% (Fig. 2C) and, consequently, in a reproducible chelate:mAb substitution ratio of about 1:1. After removal of Fe(III) by transchelation to EDTA in step 5, less than 5% iron remained complexed by mAb-*N*-sucDf after 30 min (Fig. 2D). Isolation of the mAb-*N*-sucDf on a PD-10 column efficiently removed more than 97% of EDTA, [Fe(III)EDTA]<sup>-</sup>, TFP, and *N*-sucDf (data not shown).

In step 6, mAb-*N*-sucDf was labeled with <sup>89</sup>Zr in HEPES buffer (final concentration, 0.25 mol/L) at pH 7.2–7.4. After

30 min at this pH optimum, the amount of <sup>89</sup>Zr transchelated from oxalate to mAb-*N*-sucDf is always more than 80%, even in the presence of 0.1 mol/L oxalic acid. A similar transchelation rate was found in reaction volumes of 1–9 mL, that is, enabling the use of 100–900 μL of 1 mol/L oxalic acid, provided the mAb concentration was more than 0.5 mg/mL. Below pH 6 and above pH 8, less than 15% labeling was obtained under the same conditions. The use of phosphate buffer instead of HEPES strongly affected the kinetics: At pH 7.3, the labeling efficiency was less than 30% after 30 min. Labeling efficiency was not influenced by the amount of <sup>89</sup>Zr used, in the range of 0.004–1.5 GBq. Radioimmunoconjugates could be prepared with a specific activity from 10 to 550 MBq/mg mAb. Assessment of the PD-10 column elution profile of unreacted <sup>89</sup>Zr, oxalic acid, and HEPES buffer by HPLC revealed that the compounds were quantitatively collected in the waste fractions eluted after the mAb-containing fraction.

Labeling of mmAb E48, mmAb 425, and cmAb U36 resulted in an overall yield of 80% (±6%), a radiochemical purity of more than 95% (determined with ITLC), and immunoreactive fractions of more than 90%. In general, PhosphorImager analysis of the SDS-PAGE gel revealed a major 150-kDa IgG band containing at least 93% of the radioactivity, a minor band with a higher molecular weight

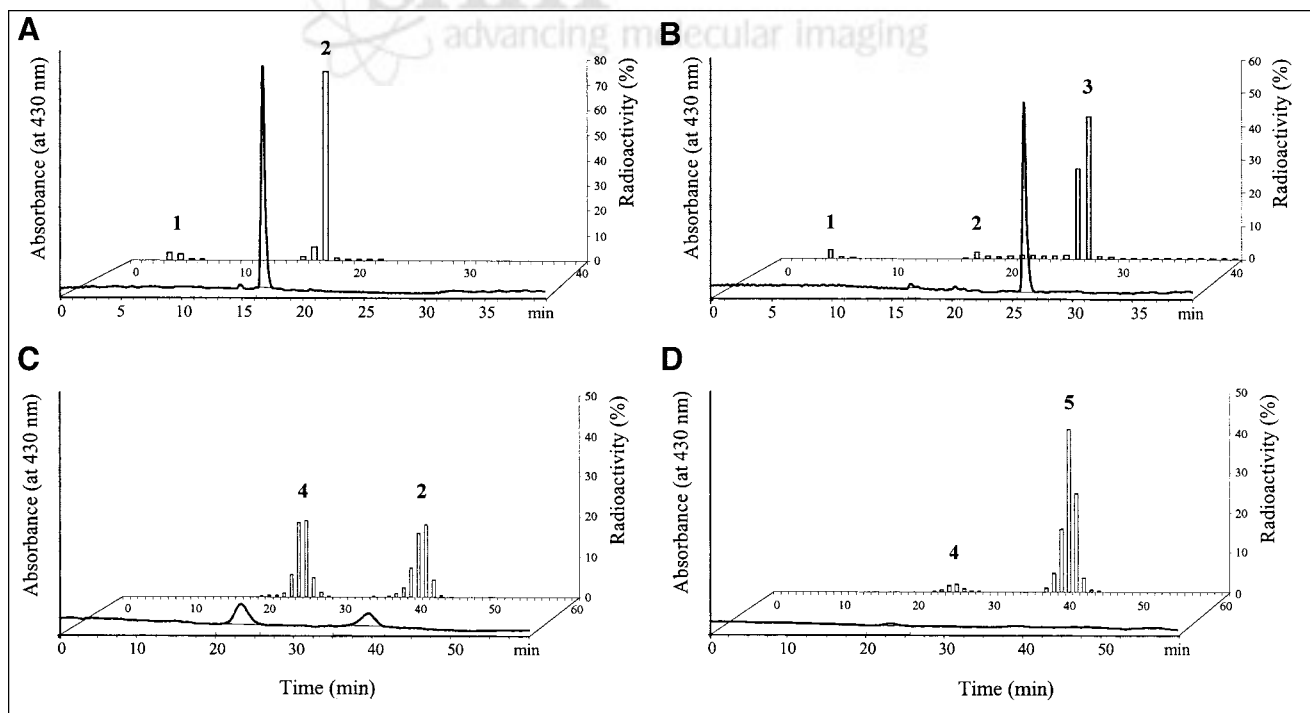


**FIGURE 2.** HPLC profiles (absorbance at 430 nm and radioactivity after fraction collection) during synthesis of TFP-*N*-sucDf ester and preparation of mAb-*N*-sucDf after reaction of *N*-sucDf with <sup>59</sup>Fe-FeCl<sub>3</sub> (A), after esterification of *N*-sucDf-<sup>59</sup>Fe-Fe (B), after reaction of TFP-*N*-sucDf-<sup>59</sup>Fe-Fe with mAb (C), and after removal of iron from mAb-*N*-sucDf-<sup>59</sup>Fe-Fe with EDTA (D). Analyses were performed with Chromspher (Chrompack) 5 C18 column (A and B) or Superdex (Pharmacia Biotech) 200 HR column (C and D). Peak 1 = unreacted <sup>59</sup>Fe-FeCl<sub>3</sub> (retention time, 3.3 min; reaction performed with an excess of 1.1 to 1); peak 2 = *N*-sucDf-<sup>59</sup>Fe-Fe (retention time, 16.7 min for A and B and 39 min for C); peak 3 = TFP-*N*-sucDf-<sup>59</sup>Fe-Fe (retention time, 25.9 min); peak 4 = mAb-*N*-sucDf-<sup>59</sup>Fe-Fe (retention time, 23 min); peak 5 = [<sup>59</sup>Fe-Fe(III)EDTA]<sup>-</sup> (retention time, 38 min).

( $\leq 3\%$ ), a minor band with a lower molecular weight ( $\leq 2\%$ ), and free  $^{89}\text{Zr}$  ( $\leq 2\%$ ). Gentisic acid was introduced during labeling and storage to prevent deterioration of the mAb integrity by radiation. The chemoprotective potency of gentisic acid (5 mg/mL, pH 5.0) was evaluated with 93 MBq  $^{89}\text{Zr}$  per milliliter as the challenging condition. Upon storage at 4°C for 2 h, 95.3% of the radioactivity was present in the 150-kDa IgG band. After 2 d, this band contained 88.7% of the radioactivity when gentisic acid was present and 79.7% when gentisic acid was absent.

#### Preparation of cmAb U36-SMCC-SATA-Df and Labeling with $^{89}\text{Zr}$

To arrive at about 1 SMCC group per mAb molecule, a SMCC/mAb molar ratio of 2 was used during the reaction. After reaction with SATA-Df and labeling with  $^{89}\text{Zr}$ , the conjugates showed a radiochemical purity of more than 95% and immunoreactive fractions of more than 90%. The overall yield was more than 80%.

#### Biodistribution in HNSCC-Bearing Nude Mice

Both radioimmunoconjugates, cmAb U36-*N*-sucDf- $^{89}\text{Zr}$  and the reference conjugate cmAb U36-SMCC-SATA-Df- $^{89}\text{Zr}$ , were injected into HNX-OE-bearing nude mice ( $n = 4$  per conjugate per time point). The conjugates had only 1 modified lysine group per mAb molecule to avoid impairment of pharmacokinetics due to overmodification (19–21). At 24, 48, and 72 h after injection, the average %ID/g (mean  $\pm$  SE) of tumor, blood, normal tissues, and gastrointestinal contents was determined (Fig. 3). Between 24 and 72 h after injection, the blood level of cmAb U36-*N*-sucDf- $^{89}\text{Zr}$  decreased from  $14.6 \pm 1.2$  to  $12.3 \pm 0.7$  %ID/g, whereas the tumor level increased from  $14.1 \pm 1.0$  to  $26.0 \pm 1.9$  %ID/g ( $P < 0.005$ ). Blood clearance of cmAb U36-SMCC-SATA-Df- $^{89}\text{Zr}$  was significantly faster: a decrease from  $10.7 \pm 0.8$  to  $5.1 \pm 0.6$  %ID/g ( $P < 0.005$ ). This enhanced blood clearance was reflected in lower tumor levels (not exceeding 10 %ID/g), lower levels in most organs, but significantly increased levels in colon content at 24 and 48 h after injection ( $4.8 \pm 0.8$  vs.  $1.7 \pm 0.2$  %ID/g,  $P < 0.05$ , and  $5.3 \pm 1.8$  vs.  $1.2 \pm 0.2$  %ID/g,  $P < 0.05$ , respectively) and in ileum content at 24 h after injection ( $1.5 \pm 0.3$  vs.  $0.5 \pm 0.2$  %ID/g,  $P < 0.05$ ).

#### In Vitro Serum Stability of cmAb U36-*N*-sucDf- $^{89}\text{Zr}$ and cmAb U36-SMCC-SATA-Df- $^{89}\text{Zr}$

The enhanced blood clearance of the reference conjugate cmAb U36-SMCC-SATA-Df- $^{89}\text{Zr}$ , as observed in vivo, was found to be related to the succinimide ring–thioether unit in the linker. Whereas HPLC analysis of cmAb U36-*N*-sucDf- $^{89}\text{Zr}$  showed no loss of radiolabel on incubation during 24 h at 37°C in human serum (Fig. 4A), the reference conjugate cmAb U36-SMCC-SATA-Df- $^{89}\text{Zr}$  gave an increased shoulder at 20 min; elution of radioactivity at 26 min, which corresponds to the HPLC retention time of albumin; and a broad radioactivity peak at 36–40 min (Fig. 4B). In a series of experiments, the nature of this phenomenon was evalu-

ated. Incubation in heat-inactivated serum gave the same results as in serum, excluding enzyme-induced instability. To verify the possible transfer of a  $^{89}\text{Zr}$ -chelate fragment to serum proteins, HSA (which contains 1 –SH group per molecule) was chosen as a representative protein. Incubation in HSA gave a pattern (data not shown) closely resembling that in Figure 4B. Increasing the pH of the HSA incubation solution to 9 resulted in a more extensive transfer of radioactivity from the monomeric mAb peak to the HSA peak, an enhanced shoulder at 20 min, and an increased peak at 36–40 min (Fig. 4C). The presence of L-cysteine reduced the transfer to HSA, with a concomitant increase in radioactivity at 39 min and a decrease in the shoulder at 20 min (Fig. 4D). Under the same conditions, mAb-*N*-sucDf- $^{89}\text{Zr}$ , as produced by the novel coupling method, did not show these instability phenomena (data not shown).

#### PET Studies

To determine the feasibility of visualizing small tumors with the novel radiolabeled cmAb U36-*N*-sucDf- $^{89}\text{Zr}$ , 12 HNX-OE-bearing nude mice were subjected to immuno-PET. In the coronal as well as transaxial images obtained at 24 h (4 mice imaged), 48 h (4 mice imaged), and 72 h (8 mice imaged) after injection, all tumors could be clearly seen as hot spots (Fig. 5). Tumors as small as 19 mg, containing about 17 kBq at the time of the scanning (72 h), could be visualized with the HRRT PET scanner. From the nontarget tissues, only the blood pool in the heart and the liver area (and nose at 24 h) was visible.

#### DISCUSSION

The assessment of tumor localizations may be improved by combining the selective tumor-targeting properties of a mAb with the excellent sensitivity and contrast resolution of PET. In the present report, we have described a novel method for labeling mAbs with the long-lived positron emitter  $^{89}\text{Zr}$  via amide bond (–NH–CO–) coupled Df, taking all the requirements for clinical application into account. Radioimmunoconjugates produced by this method were stable in serum in vitro and showed high accumulation in tumors in nude mice. The feasibility of visualizing small tumors was shown with  $^{89}\text{Zr}$  immuno-PET. The required  $^{89}\text{Zr}$  was produced in high amounts and was efficiently isolated in a consistent way.

The chelate Df has frequently been used for radiolabeling of mAbs. However, a diversity of problems was met in getting chemical control over the coupling process and the quality of the resulting final product (22–24). In the mAb-Df- $^{89}\text{Zr}$  labeling method developed by Meijs et al. (7), which was used as the reference method in the present study, lysine groups of the mAb were modified into maleimide groups, giving a succinimide ring–thioether unit in the linkage on reaction with SATA-Df. Evaluation of cmAb U36-SMCC-SATA-Df- $^{89}\text{Zr}$  prepared according to the latter method, however, revealed instability in serum in vitro, with the transfer of the  $^{89}\text{Zr}$ -chelate complex to serum

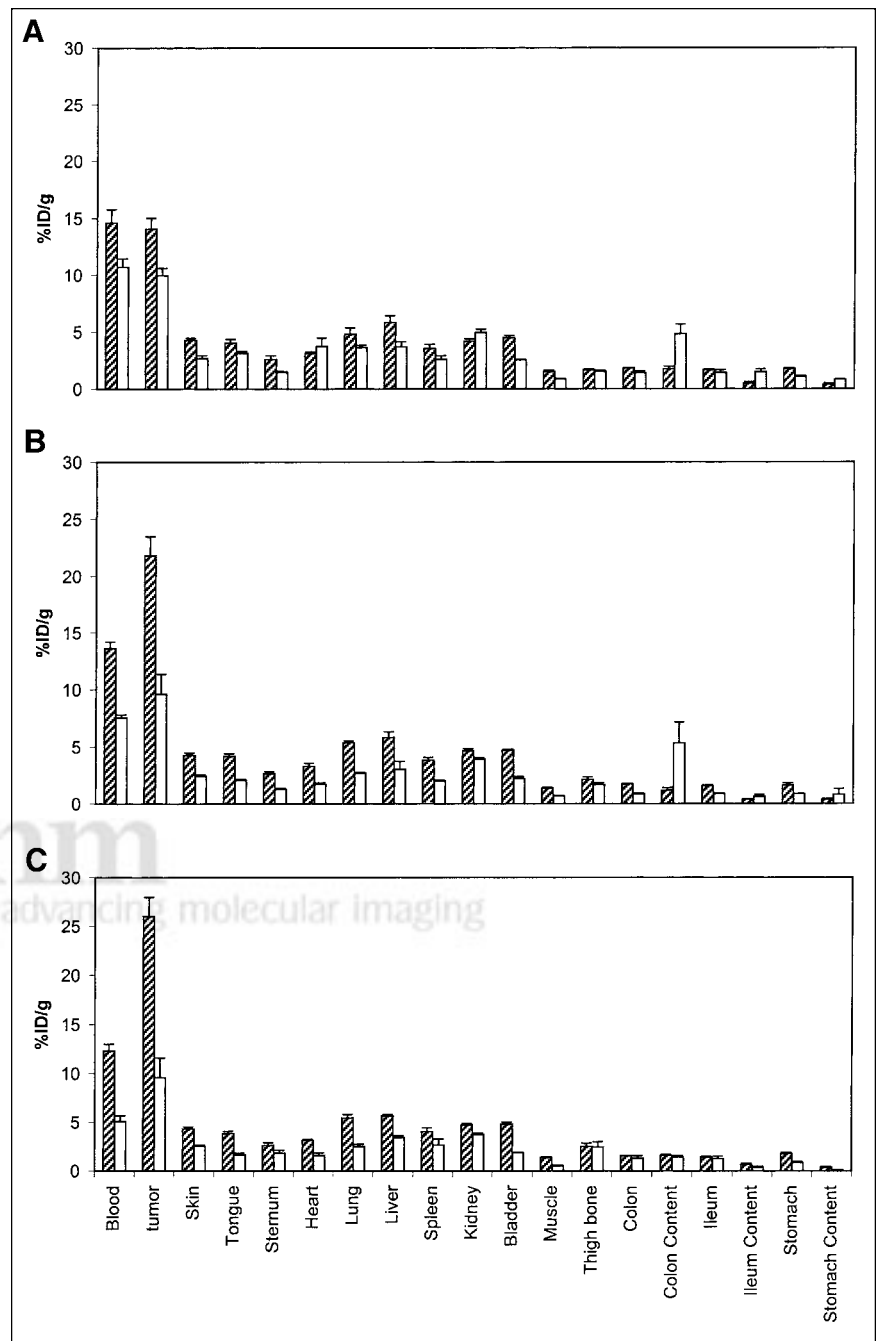


**FIGURE 3.** Biodistribution of cmAb U36-*N*-sucDf-<sup>89</sup>Zr (hatched bars, *n* = 4) and cmAb U36-SMCC-SATA-Df-<sup>89</sup>Zr (open bars, *n* = 4). Each conjugate (100 μg of mAb; 0.37 MBq) was injected into retro-orbital plexus of HNX-OE-bearing nude mice. At 24 h (A), 48 h (B), and 72 h after injection (C), mice were bled, sacrificed, and dissected, and radioactivity levels (%ID/g ± SEM) of blood, tumor, organs, and gastrointestinal contents were assessed.

proteins. In vivo experiments in tumor-bearing nude mice demonstrated such instability under physiologic conditions. Lewis and Shively (8) described comparable transfer phenomena for their <sup>90</sup>Y-DOTA-labeled mAb, containing a linker with 2 succinimide ring-thioether units. They argued a succinimide ring cleavage, possibly Y catalyzed, to be responsible for release of chelate from the mAb. Our in vitro results with HSA strongly suggest that on opening of the succinimide ring, the chelate can break off at either side of the sulfur atom (-S-). When the S-containing Df-<sup>89</sup>Zr fragment is formed, coupling with HSA takes place, while cleavage at the other side of the S-bond leaves the reactive

S-atom at the mAb side, making the mAb susceptible to aggregation (Fig. 4C). These reactions could be counteracted by quenching reactive S-atoms with L-cysteine (Fig. 4D).

To circumvent adverse in vivo instability of the mAb-Df linker, we have here described a novel coupling method based on the use of an active TFP ester. This method creates a chemically stable amide bond between the chelator Df and mAb and gives good control over the number of groups to be coupled to the mAb. To allow conjugation, the amine group present on Df was converted into a carboxylic acid functionality. For the synthesis of the corresponding TFP-

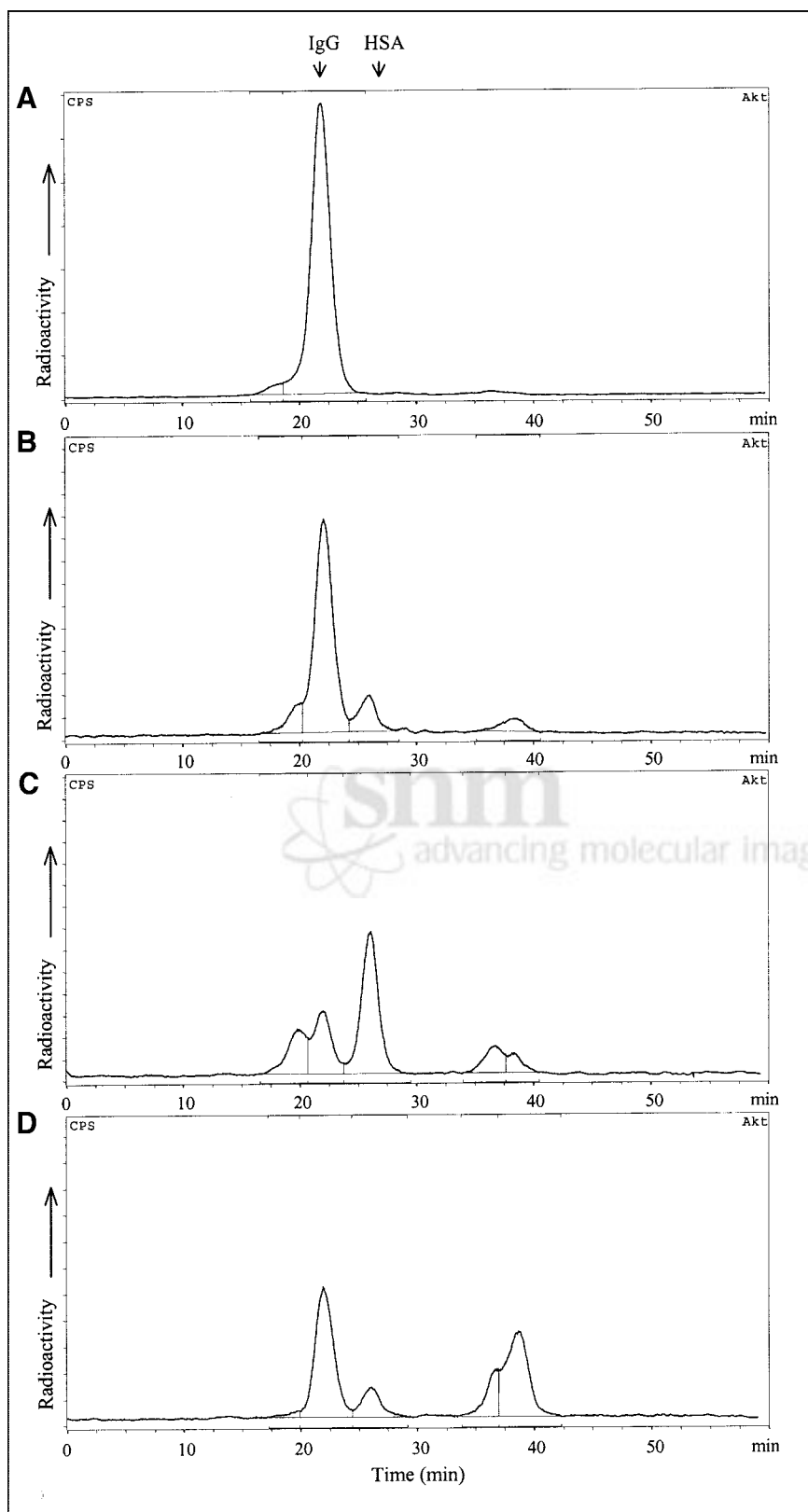


**FIGURE 4.** In vitro stability of cmAb U36-*N*-sucDf-<sup>89</sup>Zr and cmAb U36-SMCC-SATA-Df-<sup>89</sup>Zr, monitored by HPLC. Conjugates were incubated for 24 h at 37°C: cmAb U36-*N*-sucDf-<sup>89</sup>Zr in human serum (A); cmAb U36-SMCC-SATA-Df-<sup>89</sup>Zr in human serum (B); cmAb U36-SMCC-SATA-Df-<sup>89</sup>Zr in HSA, at pH 9 (C); and cmAb U36-SMCC-SATA-Df-<sup>89</sup>Zr in HSA, at pH 9 with an excess of L-cysteine (D). Retention times of IgG and HSA are indicated.

*N*-sucDf ester, it was necessary to temporarily protect the 3 hydroxamate groups of Df against reactions with EDC. Without blocking of the hydroxamate groups, intractable results were obtained that were not further analyzed. Inter-

estingly, blocking with <sup>89</sup>Zr did not yield the required TFP ester. Therefore, direct conjugation of mAbs with TFP-*N*-sucDf-<sup>89</sup>Zr was not possible. Blocking with iron proved adequate, enabling the development of a postconjugation

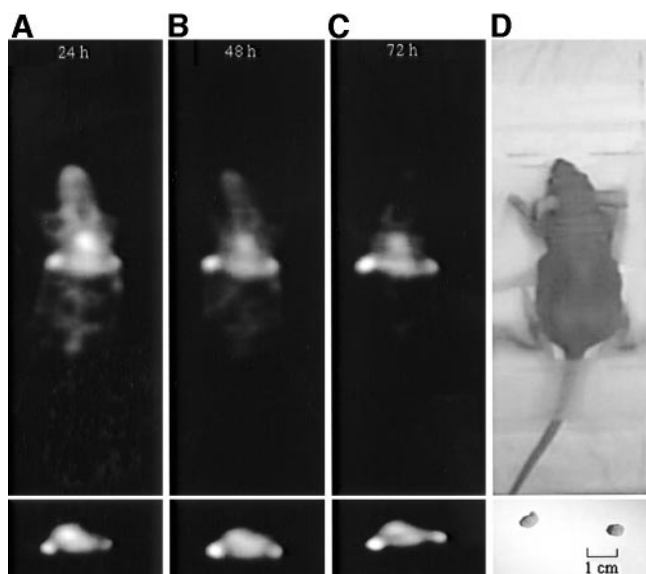


**FIGURE 5.** HNX-OE-bearing nude mouse, injected with cmAb U36-N-sucDf- $^{89}\text{Zr}$  (100  $\mu\text{g}$  of mAb; 3.7 MBq). (A–C) Coronal (upper) and transaxial (lower) PET images were obtained from same mouse at 24 h (A), 48 h (B), and 72 h (C). Image planes are those for which both tumors of same animal were visible. (D) Photographs of imaged mouse and excised tumors (left, 47 mg; right, 45 mg).

labeling method. After reaction of this TFP-N-sucDf-Fe ester with mAb, the iron was efficiently detached from Df with the aid of EDTA, under conditions that did not affect the integrity of the mAb.

For the labeling of the premodified mAb with  $^{89}\text{Zr}$ , reaction conditions were established that enabled efficient labeling in the presence of oxalic acid, the solution in which  $^{89}\text{Zr}$  is isolated. Therefore, the very time-consuming sublimation step, as proposed by Meijs et al. (12) for the removal of the potent  $^{89}\text{Zr}$ -chelating agent oxalic acid, is not required any longer. The transchelation of  $^{89}\text{Zr}$  from oxalate to Df appeared to take place efficiently within a narrow pH range (7.2–7.4). This observed sharp pH-optimum required the presence of a strong but indifferent buffer. HEPES was found to fulfill the latter requirements.

The need for protection of the mAb against radiation damage has been shown in previous mAb studies (9,25–27). Ascorbic acid as an antioxidant could not be used because this reagent causes detachment of  $^{89}\text{Zr}$  from Df by reducing  $\text{Zr}^{4+}$  to  $\text{Zr}^{2+}$ . The presence of gentisic acid during the labeling, purification, and storage proved to be beneficial and, as such, has been made part of the protocol.

Because the novel labeling procedure for  $^{89}\text{Zr}$  described in this report uses lysine residues of the mAb for the stable coupling of the Df moiety, the method is applicable to each intact mAb (as confirmed by labeling of mAbs E48 and 425), as well as to mAb fragments or peptides that contain a lysine group. The labeling of the conjugate is based on the postlabeling of a premodified mAb, which makes it possible to centrally produce sterile batches of mAb-N-sucDf, with

easy coupling of  $^{89}\text{Zr}$  at the user's site. By our strongly modified  $^{89}\text{Zr}$  isolation, it is now possible to obtain large batches of  $^{89}\text{Zr}$  (on the order of 10 GBq) in a reproducible way, at low cost, and with a radionuclidic purity of more than 99.99%.

The feasibility of visualizing small tumors with radiolabeled cmAb U36-N-sucDf- $^{89}\text{Zr}$  with an HRRT PET scanner was demonstrated in xenograft-bearing nude mice. After injection of the conjugate, HNSCC xenografts in the range of 19–154 mg were detected after 24 h. Target-to-background ratios improved when imaging was performed after prolonged periods, and none of the normal organs showed an adverse high uptake. Similar results were obtained with an ECAT EXACT HR<sup>+</sup> positron scanner (CTI) (data not shown).

Sensitive detection of small tumors in nude mice was recently also observed for the positron emitter  $^{64}\text{Cu}$  (half-life, 12.7 h) using a  $^{64}\text{Cu}$ -DOTA-minibody of T84.66 (molecular weight, 80 kDa), albeit with a high accumulation of  $^{64}\text{Cu}$  in the liver (32.4 %ID/g after 4 h) (28). With regard to  $^{124}\text{I}$ , a more suitable candidate for use in combination with whole IgG (29,30), recently the capacity of  $^{124}\text{I}$ -complementarity-determining region-grafted humanized A33 for detection of colon carcinoma xenografts in nude mice was evaluated (31,32). In this case, high-resolution images of tumors ranging from 200 to 700 mg were obtained 24 h after injection. In ongoing studies at our laboratory, we are evaluating how  $^{124}\text{I}$  compares with  $^{89}\text{Zr}$  with respect to radiopharmacokinetic behavior, tumor retention, and suitability for PET imaging of small tumors.

A direct practical clinical application of immuno-PET would be its combination with radioimmunotherapy. In this way, imaging can be used for the selection of, for example,  $^{186}\text{Re}$ -,  $^{131}\text{I}$ -, or  $^{90}\text{Y}$ -radioimmunotherapy candidates by confirmation of tumor targeting with additional estimation of radiation delivery to tumor and normal organs. The possibility of using PET with a  $^{89}\text{Zr}$ -labeled mAb to predict and quantify targeting of a  $^{90}\text{Y}$ -labeled mAb during treatment for more extended periods would be of special interest because of the lack of  $\gamma$ -emission of  $^{90}\text{Y}$ .

Because of the encouraging results presented here, the  $^{89}\text{Zr}$ -labeled cmAb U36 IgG is currently being evaluated for its capacity to detect primary tumors and metastases in operable HNSCC patients. To this end, results from  $^{89}\text{Zr}$ -immuno-PET are being compared with results from CT, MRI,  $^{18}\text{F}$ FDG PET, and histopathologic evaluation.

## CONCLUSION

This study provided practical protocols for reproducible isolation of the long-lived positron emitter  $^{89}\text{Zr}$  and its coupling to mAbs via the chelate Df using new linker chemistry. Resulting mAb- $^{89}\text{Zr}$  conjugates appeared optimal with respect to radiochemical purity, integrity, immunoreactivity, and stability. Moreover, specific targeting and sensitive detection (with a PET camera) of head and neck

cancer xenografts were demonstrated. These achievements justify clinical evaluation of mAb-<sup>89</sup>Zr conjugates.

## ACKNOWLEDGMENTS

The authors thank the staff of the BV Cyclotron (VU University) for performing the irradiations, Jan H. Rector (Solid State Physics, VU University) for sputtering <sup>89</sup>Y on copper supports, and Fred L. Buijs (Radionuclide Center, VU University) for the PET analyses.

## REFERENCES

1. Goldenberg DM, Larson SM, Reisfeld RA, Schlom J. Targeting cancer with radiolabeled antibodies. *Immunol Today*. 1995;16:261–264.
2. DeNardo SJ, Kroger LA, DeNardo GL. A new era for radiolabeled antibodies in cancer? *Curr Opin Immunol*. 1999;11:563–569.
3. de Bree R, Roos JC, Quak JJ, den Hollander W, Snow GB, van Dongen GAMS. Radioimmunoscintigraphy and biodistribution of <sup>99m</sup>Tc-labeled monoclonal antibody U36 in patients with head and neck cancer. *Clin Cancer Res*. 1995;1:591–598.
4. Colnot DR, Quak JJ, Roos JC, et al. Phase I therapy study of <sup>186</sup>Re-labeled chimeric monoclonal antibody U36 in patients with squamous cell carcinoma of the head and neck. *J Nucl Med*. 2000;41:1999–2010.
5. Sowby FD, ed. *Radionuclide Transformations: Energy and Intensity of Emissions*. ICRP publication 38, vol 11–13. Oxford, England: Pergamon Press; 1983:44, 58, 79, 205, 217, 218, 668.
6. Meijs WE, Herscheid JDM, Haisma HJ, Pinedo HM. Evaluation of desferal as a bifunctional chelating agent for labelling antibodies with zirconium-89. *Appl Radiat Isot*. 1992;43:1443–1447.
7. Meijs WE, Haisma HJ, Klok RP, et al. Zirconium-88/89 labeled monoclonal antibodies: distribution in tumour-bearing nude mice. *J Nucl Med*. 1997;38:112–118.
8. Lewis MR, Shively JE. Maleimidocysteineamido-DOTA derivatives: new reagents for radiometal chelate conjugation to antibody sulfhydryl groups undergo pH-dependent cleavage reactions. *Bioconjug Chem*. 1998;9:72–86.
9. Visser GWM, Gerretsen M, Herscheid JDM, Snow GB, van Dongen GAMS. Labeling of monoclonal antibodies with <sup>186</sup>Re using the MAG3 chelate for radioimmunotherapy of cancer: a technical protocol. *J Nucl Med*. 1993;34:1953–1963.
10. Vrouwenraets MB, Visser GWM, Stigter M, Oppelaar H, Snow GB, van Dongen GAMS. Targeting of aluminum (III) phthalocyanine tetrasulfonate by use of internalizing monoclonal antibodies: improved efficacy in photodynamic therapy. *Cancer Res*. 2001;61:1970–1975.
11. Mustafa MG, West HI, O'Brien H Jr, Lanier RG, Benhamou M, Tamura T. Measurements and a direct-reaction-plus-Hauser-Feshbach analysis of <sup>89</sup>Y(p, n)<sup>89</sup>Zr, <sup>89</sup>Y(p, 2n)<sup>88</sup>Zr, and <sup>89</sup>Y(p, pn)<sup>88</sup>Y reactions up to 40 MeV. *Physical Review C*. 1988;38:1624–1637.
12. Meijs WE, Herscheid JDM, Haisma HJ, et al. Production of highly pure no-carrier-added zirconium-89 for the labelling of antibodies with a positron emitter. *Appl Radiat Isot*. 1994;45:1143–1147.
13. Herscheid JDM, Hoekstra A, Vos C. *N*-succinyl-desferrioxamine B: a potential radiopharmaceutical for assessing renal function. *Eur J Nucl Med*. 1984;9:508–510.
14. Monzyk B, Crumbliss AL. Factors that influence siderophore-mediated iron bioavailability: catalysis of interligand iron(III) transfer from ferrioxamine B to EDTA by hydroxamic acids. *J Inorg Biochem*. 1983;19:19–39.
15. Vis RD, Kramer JLAM, Tros GHJ, van Langevelde F, Mars L. The upgraded Amsterdam nuclear microprobe. *Nucl Instrum Methods Phys Res B*. 1993;77:41–44.
16. Van Gog FB, Visser GWM, Stroomeer JWG, Roos JC, Snow GB, van Dongen GAMS. High dose rhenium-186-labeling of monoclonal antibodies for clinical application: pitfalls and solutions. *Cancer*. 1997;80:2360–2370.
17. Hermesen MAJA, Joenje H, Arwert F, et al. Centromeric breakage as a major cause of cytogenetic abnormalities in oral squamous cell carcinoma. *Genes Chromosomes Cancer*. 1996;15:1–9.
18. *Guide for the Care and Use of Laboratory Animals*. Washington, DC: Government Printing Office; 1985. NIH publication 86-23.
19. Pelegrin A, Folli S, Buchegger F, Mach JP, Wagnieres G, van den Bergh H. Antibody-fluorescein conjugates for photoimmunodiagnosis of human colon carcinoma in nude mice. *Cancer*. 1991;67:2529–2537.
20. Kukis DL, DeNardo GL, DeNardo SJ, et al. Effect of the extent of the chelate substitution on the immunoreactivity and biodistribution of 2IT-BAT-Lym-1 immunoconjugates. *Cancer Res*. 1995;55:878–884.
21. Van Gog FB, Visser GMW, Klok R, van der Schors R, Snow GB, van Dongen GAMS. Monoclonal antibodies labeled with rhenium-186 using the MAG3 chelate: relationship between the number of chelated groups and biodistribution characteristics. *J Nucl Med*. 1996;37:352–362.
22. Koizumi M, Endo K, Kunimatsu M, et al. <sup>67</sup>Ga-Labeled antibodies for immunoscintigraphy and evaluation of tumor targeting of drug-antibody conjugates in mice. *Cancer Res*. 1988;48:1189–1194.
23. Pochon S, Buchegger F, Pélegrin A, et al. A novel derivative of the chelon desferrioxamine for site-specific conjugation to antibodies. *Int J Cancer*. 1989;43:1188–1194.
24. Arano Y, Inoue T, Mukai T, et al. Discriminated release of a hippurate-like radiometal chelate in nontarget tissues for target-selective radioactivity localization using pH-dependent dissociation of reduced antibody. *J Nucl Med*. 1994;35:326–333.
25. Chakrabarti MC, Le N, Paik CH, De Graff WG, Carrasquillo JA. Prevention of radiolysis of monoclonal antibody during labeling. *J Nucl Med*. 1996;37:1384–1388.
26. Visser GW, Klok RP, Klein Gebbinck JW, ter Linden T, van Dongen GA, Molthoff CF. Optimal quality <sup>131</sup>I-monoclonal antibodies on high-dose labeling in a large reaction volume and temporarily coating the antibody with IODO-GEN. *J Nucl Med*. 2001;42:509–519.
27. Liu S, Edwards DS. Stabilization of <sup>90</sup>Y-labeled DOTA-biomolecule conjugates using gentisic acid and ascorbic acid. *Bioconjug Chem*. 2001;12:554–558.
28. Wu AM, Yazaki PJ, Tsai S, et al. High-resolution microPET imaging of carcinoembryonic antigen-positive xenografts by using a copper-64-labeled engineered antibody fragment. *Proc Natl Acad Sci*. 2000;97:8495–8500.
29. Wilson CB, Snook DE, Dhokia B, et al. Quantitative measurement of monoclonal antibody distribution and blood flow using positron emission tomography and <sup>125</sup>I-iodine in patients with breast cancer. *Int J Cancer*. 1991;47:344–347.
30. Larson SM, Pentlow KS, Volkow ND, et al. PET scanning of iodine-124-3F9 as an approach to tumor dosimetry during treatment planning for radioimmunotherapy in a child with neuroblastoma. *J Nucl Med*. 1992;33:2020–2023.
31. Lee FT, Hall C, Rigopoulos A, et al. Immuno-PET of human colon xenograft-bearing BALB/c nude mice using <sup>125</sup>I-CDR-grafted humanized A33 monoclonal antibody. *J Nucl Med*. 2001;42:764–769.
32. Eary JF. PET imaging for planning cancer therapy. *J Nucl Med*. 2001;42:770–771.